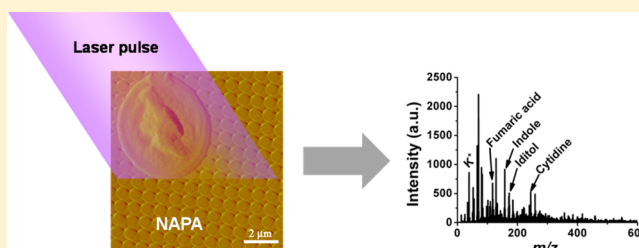# Nanophotonic Ionization for Ultratrace and Single-Cell Analysis by Mass Spectrometry

Bennett N. Walker, Jessica A. Stolee, and Akos Vertes*

W. M. Keck Institute for Proteomics Technology and Applications, Department of Chemistry, The George Washington University, Washington, District of Columbia 20052, United States

S *Supporting Information*

ABSTRACT: Recent mechanistic studies have indicated that at subwavelength post diameters and selected aspect ratios nanopost arrays (NAPA) exhibit ion yield resonances (Walker, B. N.; Stolee, J. A.; Pickel, D. L.; Retterer, S. T.; Vertes, A. *J. Phys. Chem. C* **2010**, *114*, 4835–4840). In this contribution we explore the analytical utility of these optimized structures as matrix-free platforms for laser desorption ionization mass spectrometry (LDI-MS). Using NAPA, we show that high ionization efficiencies enable the detection of ultratrace amounts of analytes (e.g., ~800 zmol of verapamil) with a dynamic range spanning up to 4 orders of magnitude. Due to the clean nanofabrication process and the lack of matrix material, minimal background interferences are present in the low-mass range. We demonstrate that LDI from NAPA ionizes a broad class of small molecules including pharmaceuticals, natural products, metabolites, and explosives. Quantitation of resveratrol in red wine samples shows that the analysis of targeted analytes in complex mixtures is feasible with minimal sample preparation using NAPA-based LDI. We also describe how multiple metabolite species can be directly detected in single yeast cells deposited on the NAPA chip. Twenty-four metabolites, or 4% of the yeast metabolome, were identified in the single-cell spectra.

M atrix-assisted laser desorption ionization (MALDI), introduced in the late 1980s, has become a mainstream ionization source for the mass spectral analysis of peptides and proteins.[1,2] Although MALDI is an efficient soft ionization method for large molecules, spectral interferences due to the applied matrix limit its use for small molecules, e.g., pharmaceuticals and metabolites. To minimize these interferences and improve sensitivity in laser desorption ionization (LDI) mass spectrometry (MS), nanoporous materials[3,4] and nanostructures, such as nanowires,[5] nanorods,[6] and nanoparticles,[2,7] have been explored. Although silicon nanowires have high aspect ratios due to their vapor–liquid–solid growth synthesis technique, they tend to be thinner and longer than the posts in nanopost arrays (NAPA). As a result they are more prone to melting and ablation at elevated laser fluences. This can result in the detection of silicon clusters in the mass spectra.[8] Laser irradiation of plasmonic structures enables ion formation from small organic adsorbates based on surface plasmon resonances.[9] As a recent comprehensive review indicates,[10] the search for a platform that exhibits high sensitivity, broad molecular coverage, and long-term stability continues. Recently proposed systems include meso- and microstructured silicon, such as nanocavities,[11] microtips,[12] and microcolumns.[13] The most broadly recognized method, desorption ionization on silicon (DIOS),[3] utilizes nanoporous silicon to trap the analyte molecules prior to laser irradiation and in some cases can achieve limits of detection down to ~800 ymol.[14] Nanoporous silicon offers high-performance characteristics with simpler fabrication than NAPA. Precise control over

the morphology of the porous structure, however, is less straightforward, and certain photonic properties, e.g., the polarization dependence of the ion yield, have not been reported.

The high sensitivity of nanostructured substrates for LDI enables the analysis of single cells. Recently, LDI-MS has been used to analyze single cells from algae[15] and to chemically image single plant[16] and mammalian cells.[4,17] These platforms can also be used to study intrapopulation heterogeneity and to better understand cell phenotypes in multicellular organisms. Typical single-cell studies have been performed on relatively large cells, with volumes exceeding 500 fL. To analyze smaller, e.g., microbial cells, ultrasensitive techniques are required.

Emerging understanding of the physical processes contributing to the LDI of adsorbates from nanostructures points to energy and plume confinement, near-field effects, and the surface properties of these substrates. For example, LDI from size-selected gold nanoparticles (AuNPs) in the ≤10 nm range showed the effect of quantum confinement on the ionization efficiency of biomolecules and peptides.[18] For silicon nanocavity arrays, a direct relationship was observed between the ion yields and the surface cavity sizes.[19] Ion production is not only dependent on the structural properties of the substrate but also on its surface chemistry.[20,21] For example, changes to the

chemistry of silicon surfaces through silylation[14] or the addition of surfactants[22] have been found to improve ionization efficiency or promote fragmentation. In nanostructure−initiator mass spectrometry (NIMS)[4] selecting the appropriate pore size, overall porosity, surface polarity, and infusing the pores with initiator compounds resulted in enhanced LDI performance.

Quasiperiodic laser-induced silicon microcolumn arrays (LISMA)[13] can be produced by the exposure of polished silicon surfaces to picosecond or femtosecond laser pulses in aqueous environments. In addition to low limits of detection, they exhibit photonic ion production, such as polarization and incidence angle-dependent ion yields.[23,24] Changing the processing environment to other liquids or gases has a limited effect on the surface morphology (e.g., column height, diameter, and periodicity) and on the arrangement of the microcolumns.[25−28] Thus, a systematic optimization of the LISMA morphology for LDI is limited by the geometries accessible through the laser surface structuring process.

Nanofabrication of silicon NAPA enables a precise control over the three crucial dimensions, height (H), diameter (D), and periodicity (P), in a wide range. Ion production on NAPA exhibits the photonic properties similar to LISMA. In addition, for NAPA with subwavelength diameter posts ion yield resonances were observed at certain aspect ratios.[29]

In this paper we explore the analytical capabilities of NAPA for a broad class of molecules varying in molecular weight, volatility, and polarity. Spectra obtained from the ionization of adsorbate molecules by NAPA exhibit minimal interferences from background ions resulting in low chemical noise. We also show that NAPA can be used for the analysis of target compounds in complex mixtures, including untreated single yeast cells.

■ EXPERIMENTAL SECTION

Nanopost Array Fabrication. The fabrication and characterization of NAPA was conducted at Oak Ridge National Laboratory, Center for Nanophase Material Sciences, and was explained in depth previously.[29] Briefly, low-resistivity p-type silicon wafers are spin-coated with resist and patterns of circles with $D = 150$ nm diameters and $P = 337$ nm periodicities are rendered on the wafer by e-beam lithography to produce patterns over 500 μm × 500 μm areas per NAPA chip. A 10 nm chromium layer is deposited onto the wafer, and nanoposts with $H = 1200$ nm height are produced by highly anisotropic reactive ion etching. The selected D, P, and H combination corresponded to the values found for a strong ion yield resonance.[29] The dimensions and uniformity of the resulting NAPA were inspected by a scanning electron microscope (SEM) (FEI, Nova Nanolab 600 DualBeam) system to verify the success of the fabrication process. An SEM image of a typical NAPA used in this study is shown in the inset of Figure 1b.

Sample Preparation. Substance P acetate salt hydrate (Arg-Pro-Lys-Pro-Gln-Gln-Phe-Phe-Gly-Leu-Met-NH$_2$), angiotensin I (Asp-Arg-Val-Tyr-Ile-His-Pro-Phe-His-Leu), bradykinin (Arg-Pro-Pro-Gly-Phe-Ser-Pro-Phe-Arg), leucine enkephalin (Tyr-Gly-Gly-Phe-Leu), verapamil, resveratrol, tenoxicam, 3-nitroaniline, loratadine, melatonin, propranolol, pseudoephedrine, ketoprofen, 1,3-dinitrobenzene, HMX (octogen), RDX (cyclonite), D-(+)-glucose solution (10%), yeast extract, peptone, yeast (*Saccharomyces cerevisiae*, type II), and HPLC grade methanol and water were purchased from Sigma-Aldrich
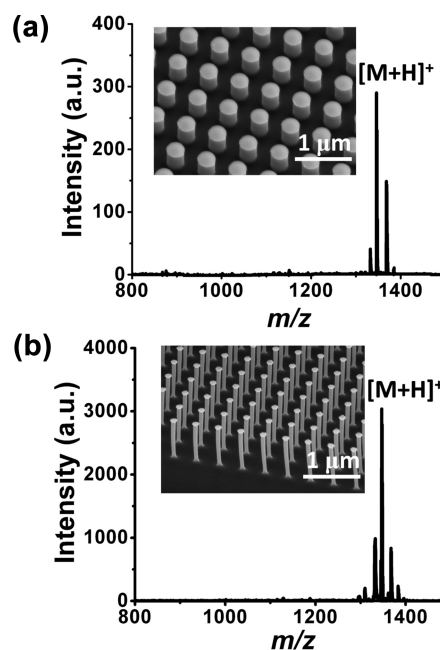

Figure 1. Comparison of positive ion LDI mass spectra of substance P from NAPA with (a) off-resonance dimensions of $H = 800$ nm post height and $D = 400$ nm post diameter, i.e., an aspect ratio of $H/D = 2$, and (b) dimensions of $H = 1000$ nm post height and $D = 100$ nm post diameter at the resonance aspect ratio of $H/D = 10$ indicate approximately 10 times higher ion yields for the latter. The amount of substance P deposited on the NAPA structures in this experiment is 1 pmol. Insets show the SEM image of the corresponding NAPA structures.

(St. Louis, MO). Serial dilutions of verapamil and resveratrol were made to determine their limits of detection and dynamic range using LDI from NAPA. Red wines were purchased from a local grocery store and, to avoid overloading the NAPA chip, diluted 1000 times in HPLC grade water before being deposited onto NAPA. Yeast were cultured by combining 10 mL of water, 2.5 mL of glucose solution, 0.25 g of peptone, 0.125 g of yeast extract, and 0.26 g of *S. cerevisiae* (type II) in a 50 mL beaker. The beaker was covered with Parafilm and incubated at 30 °C and 150 rpm for 48 h in a MaxQ 4000 shaker (Thermo Scientific, Waltham, MA).

Mass Spectrometry. Aliquots of sample solutions (0.5 μL) were deposited on the NAPA chips and allowed to air-dry. The chips were then attached to a standard MALDI plate using double-sided carbon tape. LDI-MS experiments were conducted using a curved field reflectron time-of-flight (TOF) mass spectrometer (Axima CFR, Shimadzu-Kratos, Manchester, U.K.) equipped with a 337 nm wavelength nitrogen laser. Averaged mass spectra were acquired from 100 laser shots using a 2.5 kV extraction voltage with a 100 ns delay and a 20 kV accelerating voltage. Laser pulse energies were selected just above the ionization threshold in all experiments.

Yeast Cell Deposition. Single yeast cells were deposited onto the NAPA surface using a nanospray emitter (SilicaTip, New Objective, Woburn, MA) with a 10 μm tip diameter mounted on a translation stage. The cell suspension was supplied to the emitter by a syringe pump (SP100I, WPI, Aston, U.K.). The number of cells deposited onto the NAPA chip was verified by optical microscopy. Only chips with a single yeast cell were used in the single-cell experiments. Contact mode atomic force microscopy (AFM; MPP-11100,

Veeco, Camarillo, CA) with a high aspect ratio probe tip was used to capture detailed images of the yeast cell on the NAPA surface.

■ RESULTS AND DISCUSSION

Resonance versus Off-Resonance Performance. Initially we compared the analytical performance of structures with various aspect ratios. Figure 1 depicts the SEM images of two representative structures (see the insets) and the corresponding mass spectra. The mass spectra show very low noise levels and four substance P-related peaks ([M + H − 14]$^+$, [M + H]$^+$, [M + Na]$^+$, and [M + K]$^+$). When the spectra in Figure 1a ($H = 800$ nm, $D = 400$ nm, and $H/D = 2$) and Figure 1b ($H = 1000$ nm, $D = 100$ nm, and $H/D = 10$) are compared, it is clear that the structure with the resonant aspect ratio of $H/D = 10$, in Figure 1b, produces superior ion intensities; in this case the signal is increased 10-fold. Further increasing the aspect ratio, however, leads to a dramatic drop in the ion yields. This resonant behavior is similar to the heightened response of conventional antennas at particular lengths. Varying the periodicity, however, resulted in limited or no changes in the ion yields. An important advantage of using NAPA with resonant geometry is the significantly reduced ionization threshold. The reduced fluence needed for these structures is less likely to induce fragmentation.

In the analytical applications below, we use NAPA with $D = 150$ nm and an optimum aspect ratio of $H/D = 8$. These NAPA provide slightly higher ion yields than the $D = 200$ nm posts at an optimum aspect ratio of $H/D = 6$ determined earlier.[29] SEM images after LDI experiments with the 150 nm post diameter indicate that melting does not occur. Thus, the $D = 150$ nm $H/D = 8$ system represents a sufficiently robust NAPA with high sensitivity.

Analysis of Small Molecules. The large structural and chemical diversity of small organic and biomolecules makes the development of an ion source with broad coverage difficult. Compounds with different volatilities and polarities in the molar mass range between 50 and 1500 Da were chosen for MS analysis by LDI from NAPA in positive and negative modes. Similar to LISMA, NAPA exhibits a decline in sensitivity as the analyte molecular mass approaches 2000 Da. Spectra obtained from ~1 pmol or less of verapamil, resveratrol, tenoxicam, 3-nitroaniline, loratadine, melatonin, propranolol, pseudoephedrine, ketoprofen, 1,3-dinitrobenzene, HMX, RDX, substance P, angiotensin I, bradykinin, and leucine enkephalin exhibited strong quasimolecular ion peaks and high signal-to-noise ratios in all cases. Apart from the occasional alkali ion signal, the low-mass range was devoid of chemical noise. Some examples of these spectra are shown in Figure 2.

Melatonin, a naturally occurring hormone, has a relatively low melting point of 117 °C and a low vapor pressure of unknown value. According to the NIST/EPA/NIH mass spectral library (ver. 2.0f), electron impact mass spectra of melatonin exhibit extensive fragmentation with abundant fragments at m/z 160 and 173. The NAPA-based positive ion mass spectrum of melatonin (100 fmol deposited, see Figure 2a) shows a dominant peak corresponding to the protonated molecule, potassium ion signal in the low-mass range, and a very weak potassiated melatonin peak. Although it is not utilized here, on NAPA at high laser fluences structure-specific fragment ions begin to emerge from high- and low-energy fragmentation channels.[30]
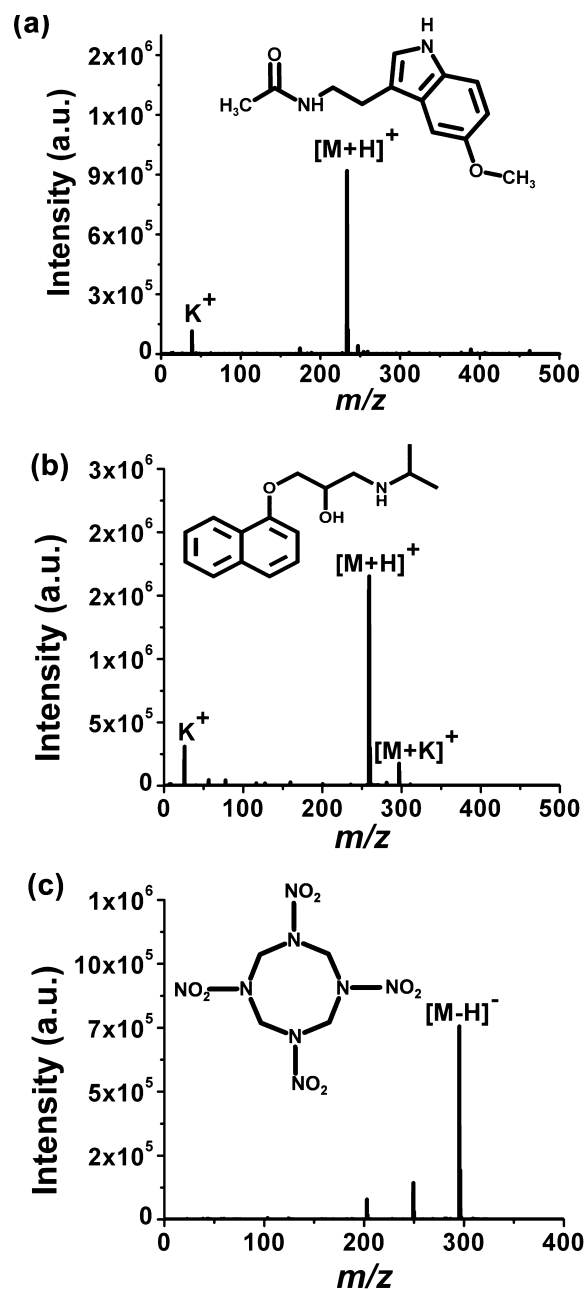

Figure 2. High signal-to-noise ratio mass spectra were acquired in positive ion mode for (a) 100 fmol of the natural hormone melatonin and (b) 100 fmol of the beta blocker propranolol, as well as for (c) 1 pmol of the high explosive HMX in negative ion mode.

The room-temperature vapor pressure and the melting point of the beta blocker propranolol are 1×10^{-8} Torr and 163 °C, respectively. The dominant peaks of the electron impact spectrum are m/z 72 and 30, with a molecular ion peak of insignificant abundance. The ionization of propranolol (see Figure 2b for the spectrum of a 100 fmol sample) and the other studied pharmaceuticals on NAPA requires lower laser fluences than peptides. This results in very clean spectra with negligible ion fragmentation. Due to their presence in solvents at trace levels, sodium and potassium ions are often observed as well as low-intensity quasimolecular sodium and potassium adducts alongside the abundant protonated molecule.

High explosives typically show elevated melting points (205 and 278 °C for RDX and HMX, respectively) and very low

vapor pressures at room temperature (3×10^{-12} and 3×10^{-15} Torr for RDX and HMX, respectively). The electron impact mass spectra of these energetic materials do not have molecular ion peaks, and the two most abundant peaks at m/z 46 and 30 do not carry structure-specific information. In contrast, the dominant peak in the negative ion mode NAPA spectrum is the molecular ion resulting from a proton loss (see the spectrum for 1 pmol of HMX in Figure 2c). Two additional minor peaks are observed due to the successive loss of two NO_2 groups.

Results on the 16 compounds from these three groups of small organics show that NAPA can be used for the detection of diverse molecules in both positive and negative mode with minimal degradation or spectral interferences.

Figures of Merit and Stability. The figures of merit were determined using verapamil, a pharmaceutical and a common test compound in mass spectrometry. A limit of detection of 800 zmol indicated the potential of NAPA-based LDI-MS for ultratrace analysis. The inset in Figure 3 shows acceptable
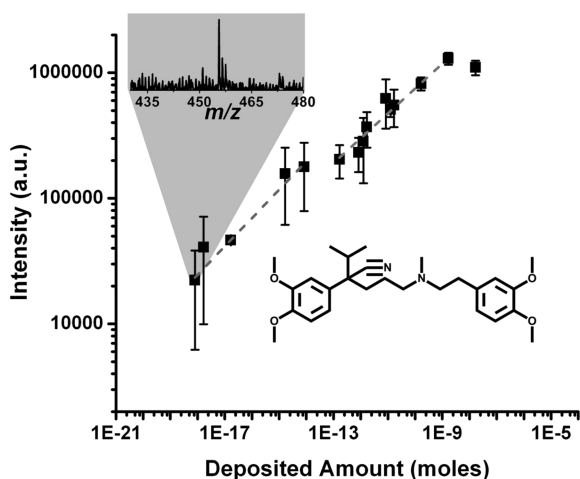

Figure 3. Molecular ion intensities for verapamil as a function of the sample amount deposited on the NAPA chip. On the basis of the mass spectra a detection limit of ~800 zmol is established. See the corresponding spectrum zoomed around the molecular ion peak in the inset. The dashed lines indicate the regressions for the two linear regions in the response curve.

signal-to-noise ratio in the molecular ion region of the mass spectrum for the limiting case. To ascertain quantitation capabilities, the dynamic range was determined by depositing various amounts of verapamil onto the NAPA chip and measuring the corresponding peak areas of the quasimolecular ions (protonated, sodiated, and potassiated) at constant laser fluence (see Figure 3). Two linear regions were observed for deposited amounts between 8×10^{-19} and 8×10^{-15} mol, as well as 2×10^{-13} and 2×10^{-9} mol. Linear regression for these two segments produces slopes of 0.23 ± 0.02 and 0.20 ± 0.01, respectively, with correlation coefficients $R^2 > 0.96$ (see the gray dashed lines in Figure 3). These attributes indicate that NAPA is especially well-suited for the analysis of severely volume-limited samples, e.g., the study of metabolites in single cells.

A possible explanation of the two linear ranges with different slopes can be based on the differences in the loading of the NAPA structure with the sample. As shown by AFM in Figure S1 of the Supporting Information, for low loading of verapamil (10^{-14} mol) the analyte is uniformly distributed in the troughs,

whereas for high loading (10^{-9} mol) uneven distribution, clumping, and analyte buildup on top of the posts are observed.

A decrease in signal intensity is observed for the highest amount of deposited verapamil (see the data point for 2×10^{-8} mol in Figure 3). This signal drop off is believed to be due to overloading the NAPA structure with the sample. AFM images (see Figure S1b of the Supporting Information) indicate that when large amounts of sample are deposited onto the NAPA structure it begins to fill in the troughs and obscure the interaction between the laser radiation and the silicon posts. This reduced interaction can result in lower levels of energy dissipation in the posts and diminished near-field enhancement of the electric field around the posts. Thus, it is important to remember that the overall sample capacity of these NAPA chips is approximately 2 nmol.

To assess the long-term stability of the NAPA structures, chips were stored in low-humidity environment for 7 months. Comparison of mass spectra before and after the extended storage (not shown) indicated no significant decrease in ionization efficiency. A slight increase in the spectral noise level, however, was noticed. A likely source of the increased noise is contamination during storage. These results suggest that the nanopost performance degradation during extended storage is negligible.

Although NAPA structures are intended to be disposed of after a single use, we have found that, with proper cleaning, i.e., rinsing with methanol and water followed by sonication, they can be reused for additional analyses. This is especially true at analyte concentrations above the ultratrace levels. Inspection of the NAPA structures by SEM imaging indicates the lack of structural damage on the nanoposts after laser irradiation at fluence levels close to the ion generation threshold. This helps with the reusability of NAPA and the shot-to-shot stability of the signal during the LDI-MS experiments.

Analysis of Mixtures. As most analytical problems involve complex mixtures rather than pure samples, it is important to explore potential interferences and ion suppression effects. For example, peptide mixtures are commonly analyzed in proteomics applications. A mass spectrum from an equimolar peptide mixture containing 1 pmol amounts of leucine enkephalin, bradykinin, angiotensin I, and substance P, each, deposited onto a NAPA chip is shown in Figure 4a. All of the components are present as intact quasimolecular ions, although not with equal intensities. The response from angiotensin I is significantly weaker than from the other peptides, especially if we take into account the intensities of the two fragment ions, x_1 from leucine enkephalin and a_3 from substance P. The isotope ion peaks in the inset are well-resolved, and their intensities closely resemble the calculated isotope distribution of substance P.

Quantitation of targeted compounds in complex mixtures is another task commonly performed in, e.g., food or environmental analysis. For example, recent investigations have found a correlation between a reduction in cardiovascular and cerebrovascular risks and a moderate consumption of red wine.[31,32] These studies claimed that resveratrol, a stilbenoid with a monoisotopic mass of 228.079 Da, and proanthocyanidin in the wine helped to maintain cardiac health and could increase life expectancy. Thus, it became important to rapidly profile resveratrol and other compounds in commercial wines[33] and to follow the transformations of resveratrol in human metabolism.[34] Representative concentrations of *trans*-resveratrol in red wine range between 0.4 and 63 μM,[31,35] and its
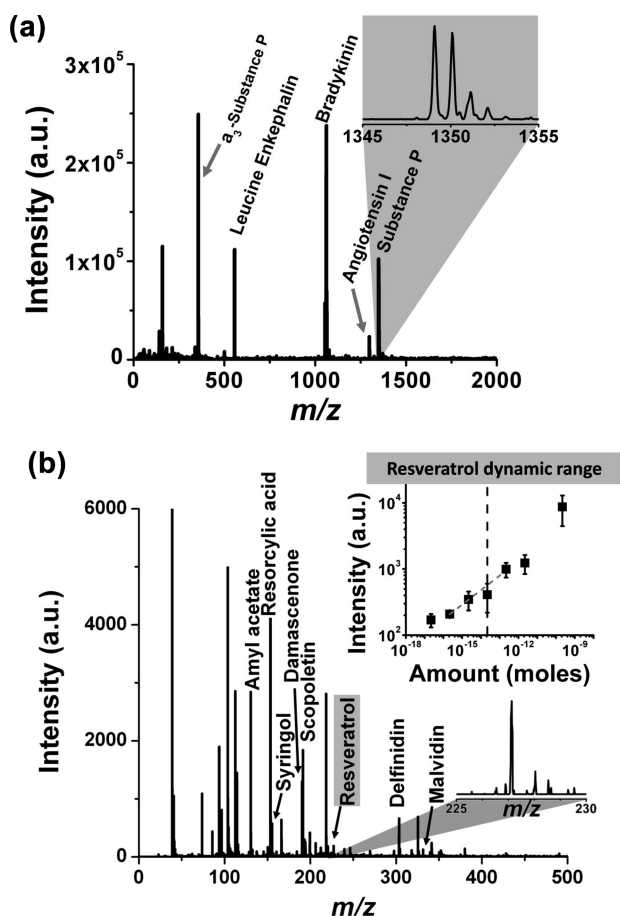
(a)

(b)

Figure 4. (a) Positive ion LDI mass spectrum of a four-peptide mixture containing leucine enkephalin, bradykinin, angiotensin I, and substance P from NAPA shows the molecular ion peaks and two known fragments. The inset shows the isotope distribution pattern of the protonated substance P molecule. (b) Negative ion LDI mass spectrum of red wine from NAPA. Ten of the 15 putatively assigned compounds, including resveratrol, are labeled. The zoomed spectrum in the range of the isotope distribution pattern for resveratrol is in the bottom inset. The top inset depicts the quantitative LDI response from NAPA for a wide range of deposited resveratrol amounts. The values determined for red wine (vertical dashed line) are well within the range of quantitation (fitted dashed line in gray).

quantitation typically requires a separation step followed by negative ion electrospray MS.[36] Due to the presence of hundreds of compounds in wine samples, the identification of resveratrol through MS relies on accurate mass measurements, the determination of isotope distribution, and ultimately, fragmentation studies.

To prevent overloading the NAPA chip by the abundant components of the wine, a 1000-times dilution in water was performed before analysis. To obtain the LDI mass spectrum of red wine, 0.5 μL of the diluted sample was deposited on a NAPA. A typical negative ion spectrum, shown in Figure 4b, contains ~100 peaks. Fifteen of them, including resveratrol, are putatively identified based on accurate masses within a $\pm$ 6 mDa margin, addition of resveratrol standard to the sample, isotope distribution patterns (see the bottom inset in Figure 4b), and information from previous studies.[32,33,37,38] To establish the figures of merit for resveratrol analysis on NAPA, standard samples were analyzed in a wide range of concentrations. The top inset in Figure 4b shows the peak

intensity as a function of the deposited moles of resveratrol in the 2×10^{-17} to 2×10^{-10} mol range. On the basis of this data, a detection limit of 20 amol was established with a 3 orders of magnitude range of quantitation between 2×10^{-16} and 2×10^{-13} mol. Linear regression in this range yielded a correlation coefficient of R^2 = 0.95. From this curve, a combined concentration of *cis-* and *trans-*resveratrol of ~68 μM was found for the studied red wine samples, which is within the margin of error for the high values found in the literature.[31]

Single-Cell Analysis. Detection of metabolites from single microbial cells requires highly sensitive multispecies techniques.[39] The estimated amounts of primary metabolites within a budding yeast (*S. cerevisiae*) cell, with a volume of only 30 fL, are typically between 10 amol and 30 fmol.[40] On the basis of its figures of merit, LDI-MS from NAPA is expected to be sufficiently sensitive for producing mass spectra in this range. As the yeast metabolic network is relatively small and has been thoroughly analyzed,[40] the identification of metabolites is relatively simple.

Single yeast cells were directly deposited onto NAPA chips and analyzed by LDI-MS in positive and negative ion mode. Figure 5a shows an AFM image of a yeast cell on a NAPA structure before laser exposure. During LDI, laser excitation of the posts ruptures the cell, exposing and ionizing the intracellular components. Figure 5b, shows a representative
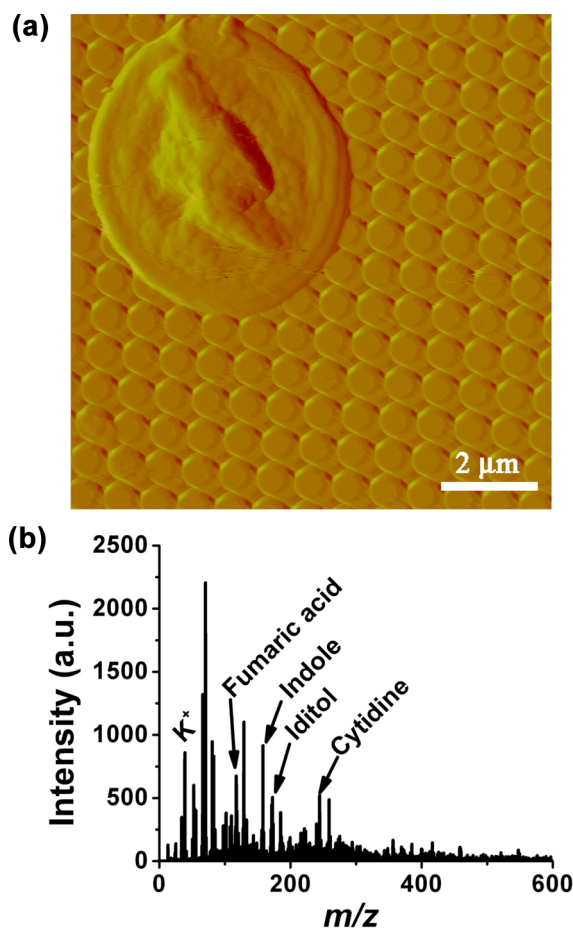
(a)

(b)

Figure 5. (a) Atomic force microscope image of a single yeast cell deposited on a NAPA before LDI-MS analysis. (b) LDI mass spectrum of a single yeast cell from NAPA in the mass range of metabolites. Four of the ~24 putatively assigned metabolites are labeled.

Table 1. Metabolites Detected in a Single Yeast Cell by LDI from NAPA

no.	assigned metabolite	ion	calcd m/z	measd m/z	Δ m/z
1	amino propanol	[M − H]⁻	74.061	74.048	0.013
2	isobutyrate/acetoin	[M − H]⁻	87.040	87.033	0.007
3	cadaverine	[M + H]⁺	103.136	103.132	0.004
4	proline	[M + H]⁺	116.053	116.071	−0.018
5	fumaric acid	[M + H]⁺	117.019	117.010	0.009
6	aspartate semialdehyde/amino oxobutanoate	[M + H]⁺	118.050	117.990	0.060
7	threonine/homoserine	[M + K]⁺	158.060	158.021	0.039
8	threonine/homoserine	[M + H]⁺	120.066	120.035	0.031
9	glutamic semialdehyde/aminolevulinate/aminooxopentanoate	[M + H]⁺	132.066	132.030	0.036
10	methionine	[M − H]⁻	148.040	148.070	−0.030
11	xanthine/xylitol	[M − H]⁻	151.026	151.050	−0.024
			151.060		
12	indole/valine/aminopentanoate	[M + K]⁺	156.021	156.050	−0.029
			156.043		
13	dihydroxyacetone phosphatidic acid/glyceraldehyde phosphate/phospholactate/sulfolactate	[M + H]⁺	171.005	170.996	0.009
			171.005		
			171.005		
			170.997		
14	glycerol phosphatidic acid/dehydroshikimate	[M + H]⁺	173.022	173.021	0.022
			173.045		
15	histidinol	[M + K]⁺	180.037	180.052	−0.015
16	iditol	[M + H]⁺	183.086	183.097	−0.011
17	phosphohomoserine	[M + H]⁺	200.030	200.060	−0.030
18	lipoamide	[M + H]⁺	206.067	206.093	−0.026
19	pantothenate	[M − H]⁻	218.103	218.122	−0.019
20	cytidine	[M + H]⁺	244.093	244.040	0.053
21	inosine	[M − H]⁻	267.070	267.090	−0.020
22	naringenin	[M − H]⁻	271.061	271.023	0.038
23	sedoheptulose phosphatidic acid	[M + H]⁺	290.160	290.101	0.059
24	phosphoribosylformylglycineamidine	[M + H]⁺	314.075	314.070	0.005

mass spectrum from a single-cell experiment with some of the assigned metabolites. Initially multicell spectra were acquired for identification of the peaks with higher fidelity. On the basis of the spectra for multiple cells, accurate mass measurements, isotope distribution patterns, literature data, and database searches[41] were used to assign the peaks. In total, 24 biochemicals, corresponding to ~4% of the known metabolome, were detected (see Table 1). On the basis of these assignments, the coverage of major biochemical pathways was 29% with at least one metabolite in a pathway identified. In one example, 5 out of 12 metabolites involved in the threonine and methionine biosynthesis superpathway were assigned. Detailed direct analysis of single cells with LDI from NAPA can improve our understanding of how individual cells grow, develop, and respond to environmental stress, as well as reveal the metabolites involved in chemical communication between cells.

■ CONCLUSIONS

Mechanistic studies on NAPA structures, a representative of nanophotonic ion sources, indicated the existence of select geometries that produce a resonance-like enhancement in ion yields. In this contribution, LDI on NAPA with a resonant structure is shown to enable the ultratrace level detection of small molecules in the mass range between 50 and 1500 Da. Limits of detection for verapamil and resveratrol are established at 800 zmol and 20 amol, respectively. A comparison of LISMA and NAPA indicates improved figures of merit for the latter. For example, typical limit of detection for LISMA was 10 fmol for the P14R synthetic peptide. Quantitation with the most

commonly used LDI method, MALDI, is only possible in a narrow range of concentrations. With NAPA we show a dynamic range of 3−4 orders of magnitude for resveratrol and verapamil. On the basis of investigating spectral responses from 16 compounds, NAPA promises to be a robust LDI platform for the analysis of a broad range of small molecules including pharmaceuticals, natural products, explosives, and metabolites. Initial stability experiments indicate unchanged LDI performance for at least 7 months of storage in a low-humidity environment. The most significant disadvantage of the NAPA platform is its involved fabrication. It requires a nanofabrication facility in a clean room. This process, however, confers a valuable advantage, i.e., the extremely low chemical background due to the clean fabrication environment.

Turning to real-world samples, we show examples of detecting and quantitating targeted compounds in complex mixtures. Resveratrol is readily detected in red wine without the need for a separation method. After depositing a drop of diluted red wine on a NAPA chip, we obtain an negative ion LDI spectrum exhibiting ~100 peaks and determine the combined concentration of cis- and trans-resveratrol. In another example, a severely volume-limited sample is analyzed on NAPA. A single yeast cell with a typical volume of ~30 fL is sufficient to produce a complex LDI spectrum. In these spectra we are able to tentatively assign 24 metabolites, which correspond to a 4% coverage of the yeast metabolome. Metabolite profiling of single cells opens the door to studying cellular heterogeneity, a crucial step in understanding cell-to-cell variations in physiology and environmental response. A

crucial step in entering that field is to develop high-throughput capabilities for the NAPA-based analytical platforms. Experiments to analyze single mammalian cells on NAPA are underway and will be reported in a separate contribution.

ASSOCIATED CONTENT

Supporting Information

Additional information as noted in text. This material is available free of charge via the Internet at http://pubs.acs.org.

AUTHOR INFORMATION

Corresponding Author

*E-mail: vertes@gwu.edu. Phone: +1 202-994-2717. Fax: +1 202-994-5873.

Notes

The authors declare no competing financial interest.

ACKNOWLEDGMENTS

REFERENCES

(1) Karas, M.; Hillenkamp, F. *Anal. Chem.* **1988**, *60*, 2299−2301.

(2) Tanaka, K.; Waki, H.; Ido, Y.; Akita, S.; Yoshida, Y.; Yoshida, T. *Rapid Commun. Mass Spectrom.* **1988**, *2*, 151−153.

(3) Wei, J.; Buriak, J. M.; Siuzdak, G. *Nature* **1999**, *399*, 243−246.

(4) Northen, T. R.; Yanes, O.; Northen, M. T.; Marrinucci, D.; Uritboonthai, W.; Apon, J.; Golledge, S. L.; Nordstrom, A.; Siuzdak, G. *Nature* **2007**, *449*, 1033−1036.

(5) Go, E. P.; Apon, J. V.; Luo, G.; Saghatelian, A.; Daniels, R. H.; Sahi, V.; Dubrow, R.; Cravatt, B. F.; Vertes, A.; Siuzdak, G. *Anal. Chem.* **2005**, *77*, 1641−1646.

(6) Castellana, E. T.; Gamez, R. C.; Gomez, M. E.; Russell, D. H. *Langmuir* **2010**, *26*, 6066−6070.

(7) Wen, X. J.; Dagan, S.; Wysocki, V. H. *Anal. Chem.* **2007**, *79*, 434−444.

(8) Luo, G. H.; Chen, Y.; Daniels, H.; Dubrow, R.; Vertes, A. *J. Phys. Chem. B* **2006**, *110*, 13381−13386.

(9) Owega, S.; Lai, E. P. C.; Bawagan, A. D. O. *Anal. Chem.* **1998**, *70*, 2360−2365.

(10) Stolee, J. A.; Walker, B. N.; Zorba, V.; Russo, R. E.; Vertes, A. *Phys. Chem. Chem. Phys.* **2012**, *14*, 8453−8471.

(11) Xiao, Y. S.; Retterer, S. T.; Thomas, D. K.; Tao, J. Y.; He, L. *J. Phys. Chem. C* **2009**, *113*, 3076−3083.

(12) Gorecka-Drzazga, A.; Dziuban, J.; Drzazga, W.; Kraj, A.; Silberring, J. *J. Vac. Sci. Technol., B* **2005**, *23*, 819−823.

(13) Chen, Y.; Vertes, A. *Anal. Chem.* **2006**, *78*, 5835−5844.

(14) Trauger, S. A.; Go, E. P.; Shen, Z. X.; Apon, J. V.; Compton, B. J.; Bouvier, E. S. P.; Finn, M. G.; Siuzdak, G. *Anal. Chem.* **2004**, *76*, 4484−4489.

(15) Amantonico, A.; Urban, P. L.; Fagerer, S. R.; Balabin, R. M.; Zenobi, R. *Anal. Chem.* **2010**, *82*, 7394−7400.

(16) Holscher, D.; Shroff, R.; Knop, K.; Gottschaldt, M.; Crecelius, A.; Schneider, B.; Heckel, D. G.; Schubert, U. S.; Svatos, A. *Plant J.* **2009**, *60*, 907−918.

(17) Rubakhin, S. S.; Romanova, E. V.; Nemes, P.; Sweedler, J. V. *Nat. Methods* **2011**, *8*, S20−S29.

(18) McLean, J. A.; Stumpo, K. A.; Russell, D. H. *J. Am. Chem. Soc.* **2005**, *127*, 5304−5305.

(19) Finkel, N. H.; Prevo, B. G.; Velev, O. D.; He, L. *Anal. Chem.* **2005**, *77*, 1088−1095.

(20) Kruse, R. A.; Li, X. L.; Bohn, P. W.; Sweedler, J. V. *Anal. Chem.* **2001**, *73*, 3639−3645.

(21) Thomas, J. J.; Shen, Z. X.; Crowell, J. E.; Finn, M. G.; Siuzdak, G. *Proc. Natl. Acad. Sci. U.S.A.* **2001**, *98*, 4932−4937.

(22) Nordstrom, A.; Apon, J. V.; Uritboonthal, W.; Go, E. P.; Siuzdak, G. *Anal. Chem.* **2006**, *78*, 272−278.

(23) Walker, B. N.; Razunguzwa, T.; Powell, M.; Knochenmuss, R.; Vertes, A. *Angew. Chem., Int. Ed.* **2009**, *48*, 1669−1672.

(24) Stolee, J. A.; Walker, B. N.; Chen, Y.; Vertes, A. *AIP Conf. Proc.* **2010**, *1278*, 98−110.

(25) Her, T. H.; Finlay, R. J.; Wu, C.; Mazur, E. *Appl. Phys. A: Mater. Sci. Process.* **2000**, *70*, 383−385.

(26) Wu, C.; Crouch, C. H.; Zhao, L.; Carey, J. E.; Younkin, R.; Levinson, J. A.; Mazur, E.; Farrell, R. M.; Gothoskar, P.; Karger, A. *Appl. Phys. Lett.* **2001**, *78*, 1850−1852.

(27) Pedraza, A. J.; Fowlkes, J. D.; Guan, Y. F. *Appl. Phys. A: Mater. Sci. Process.* **2003**, *77*, 277−284.

(28) Crouch, C. H.; Carey, J. E.; Warrender, J. M.; Aziz, M. J.; Mazur, E.; Genin, F. Y. *Appl. Phys. Lett.* **2004**, *84*, 1850−1852.

(29) Walker, B. N.; Stolee, J. A.; Pickel, D. L.; Retterer, S. T.; Vertes, A. *J. Phys. Chem. C* **2010**, *114*, 4835−4840.

(30) Stolee, J. A.; Vertes, A. *Phys. Chem. Chem. Phys.* **2011**, *13*, 9140−9146.

(31) Baur, J. A.; Sinclair, D. A. *Nat. Rev. Drug Discovery* **2006**, *5*, 493−506.

(32) Bertelli, A. A. A.; Das, D. K. *J. Cardiovasc. Pharmacol.* **2009**, *54*, 468−476.

(33) Carpentieri, A.; Marino, G.; Amoresano, A. *Anal. Bioanal. Chem.* **2007**, *389*, 969−982.

(34) Yu, C. W.; Shin, Y. G.; Chow, A.; Li, Y. M.; Kosmeder, J. W.; Lee, Y. S.; Hirschelman, W. H.; Pezzuto, J. M.; Mehta, R. G.; van Breemen, R. B. *Pharm. Res.* **2002**, *19*, 1907−1914.

(35) Goldberg, D. M.; Ng, E.; Karumanchiri, A.; Diamandis, E. P.; Soleas, G. *J. Am. J. Enol. Vitic.* **1996**, *47*, 415−420.

(36) Careri, M.; Corradini, C.; Elviri, L.; Nicoletti, I.; Zagnoni, I. *J. Agric. Food Chem.* **2004**, *52*, 6868−6874.

(37) Mazzuca, P.; Ferranti, P.; Picariello, G.; Chianese, L.; Addeo, F. *J. Mass Spectrom.* **2005**, *40*, 83−90.

(38) Alcalde-Eon, C.; Escribano-Bailon, M. T.; Santos-Buelga, C.; Rivas-Gonzalo, J. C. *Anal. Chim. Acta* **2006**, *563*, 238−254.

(39) Amantonico, A.; Oh, J. Y.; Sobek, J.; Heinemann, M.; Zenobi, R. *Angew. Chem., Int. Ed.* **2008**, *47*, 5382−5385.

(40) Forster, J.; Famili, I.; Fu, P.; Palsson, B. O.; Nielsen, J. *Genome Res.* **2003**, *13*, 244−253.

(41) *Saccharomyces* Genome Database. http://www.yeastgenome.org (accessed July 29, 2012).

7762

dx.doi.org/10.1021/ac301238k | *Anal. Chem.* 2012, 84, 7756−7762

Supporting Information for

Nanophotonic Ionization for Ultratrace and Single-Cell Analysis by Mass Spectrometry
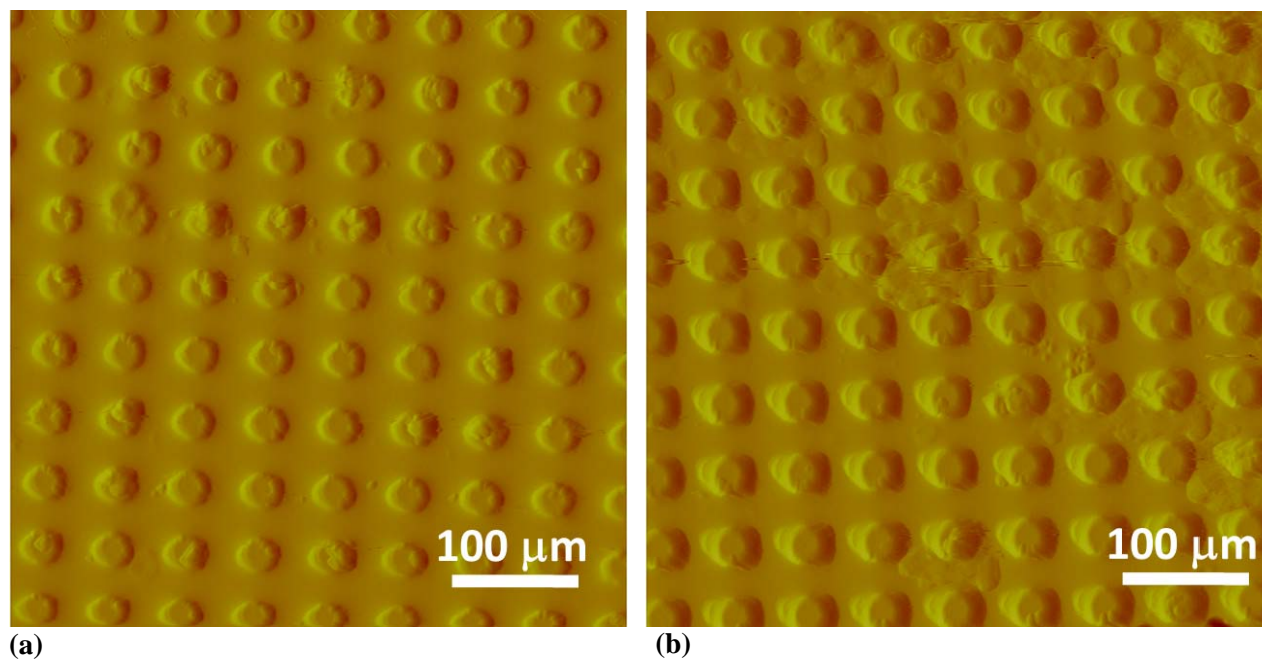
Bennett N. Walker, Jessica A. Stolee, and Akos Vertes*

W. M. Keck Institute for Proteomics Technology and Applications, Department of Chemistry,

The George Washington University, Washington, District of Columbia 20052, United States

* To whom correspondence should be addressed. E-mail: vertes@gwu.edu. Phone: +1 (202) 994-2717.

Fax: +1 (202) 994-5873.

Figure S1. Atomic force microscope image of analyte distributions in NAPA structures. For (a) low loading of verapamil (e.g., 10^{-14} moles) the analyte is uniformly distributed in the troughs, whereas for (b) high loading (e.g., 10^{-9} moles) uneven distribution, clumping and analyte buildup on top of the posts are observed.

(a)　　　　　　　　　　　　　　　　　　(b)

ACKNOWLEDGMENTS